EASR

Engineering and Applied Science Research

https://www.tci-thaijo.org/index.php/easr/index

Published by the Faculty of Engineering, Khon Kaen University, Thailand

Modeling standard lines for soil compaction testing using artificial neural networks and geometric algorithms

Anan Butrat[1)] and Rattanachot Thongpong*[2)]

[1)]Department of Industrial Management Engineering, Faculty of Industrial Technology, Valaya Alongkorn Rajabhat University under the Royal Patronage Pathum Thani Province, Pathum Thani 13180, Thailand
[2)]Department of Civil Engineering Technology, Faculty of Industrial Technology, Valaya Alongkorn Rajabhat University under the Royal Patronage Pathum Thani Province, Pathum Thani 13180, Thailand

Received 10 January 2025
Revised 9 May 2025
Accepted 23 May 2025

Abstract

Soil compaction testing is crucial for ensuring the stability and durability of infrastructure projects. Traditional methods for generating standard lines, such as averaging and polynomial fitting, often fail to capture the nonlinear relationships and variability in compaction data, leading to inaccuracies in soil property assessments. This study introduces a novel framework that leverages Artificial Neural Networks (ANNs) to dynamically model standard lines for compaction curves, addressing limitations of traditional approaches. Four activation functions—ReLU, Sigmoid, Tanh, and Swish—were evaluated, with Swish emerging as most effective for capturing complex relationships between Dry Density (DD) and Moisture Content (MC). A tolerance-based evaluation framework, incorporating tolerance levels of 2%, 5%, and 10%, was applied to analyze coverage areas. The 5% tolerance level was identified as most balanced, minimizing errors while providing reliable representations of compaction data. The study also introduced the Ray-Casting Algorithm for precise calculation of coverage areas, enabling a new performance indicator based on density of data points within the region. Results demonstrate that the ANN framework, particularly with Swish activation, outperforms traditional statistical methods in accuracy and adaptability. ReLU delivered the best performance, with the lowest prediction and percentage errors (0.1910–0.2005 and 10.66%–11.74%), while effectively explaining over 55% of the data's variability. Sigmoid showed the weakest results, with high errors and near-zero variance explanation. Tanh performed moderately, balancing accuracy and generalization with reasonable error levels and 44%–54% variance capture. Swish was consistently reliable, with stable errors and over 50% of the variance explained. This research advances compaction testing by addressing variability, operator-induced errors, and nonlinear data patterns, establishing a reliable methodology for generating standard lines. Future work could explore diverse soil types, integrate environmental factors, develop hybrid machine learning models, and improve performance indicators.

Keywords: Soil compaction testing, Artificial Neural Networks (ANNs), Standard line generation, Ray-Casting Algorithm, Tolerance-Based Evaluation, Geotechnical engineering

1. Introduction

Soil compaction testing plays a critical role in geotechnical engineering, ensuring the stability and durability of infrastructure projects. This process typically involves determining the relationship between soil density and moisture content to achieve the Maximum Dry Density (MDD) at the Optimum Moisture Content (OMC). The compaction curve generated during testing provides valuable insights into soil behavior. However, errors in compaction test results, whether due to operator variability, equipment calibration, or environmental factors, can lead to discrepancies in the compaction curves, ultimately impacting the reliability of soil assessments. Studies such as [1], [2], and [3] have highlighted how variability in soil composition, environmental conditions, and operator-induced errors can influence compaction results, emphasizing the need for more robust testing methods.

To address these inconsistencies, current methodologies often focus on generating a standard line to represent a set of compaction curves as a single unified profile. This approach is crucial for standardizing compaction results across different tests and operators. The most commonly used methods for creating a standard line include averaging compaction curves and fitting polynomial equations to represent the data, as shown in Figure 1. Averaging methods, as explored by [4], aim to create a baseline by calculating the mean compaction curve across multiple tests, while polynomial fitting methods, discussed by [5] and [6], attempt to represent the overall trend of compaction data through mathematical models. While these methods provide a simplified representation, they may not fully capture the variability and nuances of the underlying compaction data. Recent studies, including [7], [8], and [9], have explored these statistical and computational methods for standard line generation, but significant gaps remain in their ability to handle diverse datasets effectively.

Artificial Neural Networks (ANNs) have demonstrated their capability in handling complex datasets and identifying patterns in diverse applications. Their ability to model nonlinear relationships and generalize across varying conditions makes them a promising

*Corresponding author.
Email address: rattanachot.thong@vru.ac.th
doi: 10.14456/easr.2025.39

tool for creating a standard line of compaction curves. By training ANNs on compaction test data, it is possible to generate a representative standard line that minimizes errors and accounts for variability in the dataset. Research by [10], [11], and [12] has shown the potential of ANNs in geotechnical applications, including soil property predictions and compaction analysis, providing a strong foundation for this approach.

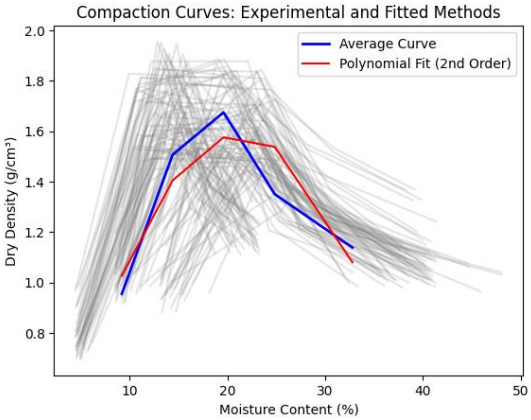

Figure 1 Standard curve by traditional approaches

The performance of a standard line can be evaluated through specific indicators, such as the coverage area created by a ± tolerance band around the standard line, which reflects the consistency and reliability of the compaction data. However, traditional methods of evaluating coverage area often lack precision. This study introduces the Ray-Casting Algorithm as an innovative approach to calculate the coverage area and proposes a new performance indicator that incorporates the density of data points within the coverage region. Studies by [13], [14], and [15] have explored similar geometric algorithms in spatial data analysis, but their application to soil compaction testing represents a novel direction.

Table 1 Summary of recent studies about ANN and ML

Reference / Study	Soil Compaction Prediction (ML/ANN)	Comparison of ML Models	Explainable AI / Sensitivity Analysis	Focus on Standard Line Creation	Geometric Algorithm / Ray-Casting	New Indicator / Evaluation Method
Gurtug et al. [7]	X (Statistical prediction)			✓ (Standardization issues discussed)		
Khatti and Grover [16]	✓	✓				
Othman and Abdelwahab [3]	✓ (Deep neural networks)					
Khatti and Grover [17]	✓	✓ (LSSVM, LSTM, LSBoostRF, ANN)				
Khatti and Grover [18]	✓	✓ (multiple soft computing models)				
Khatti and Grover [19]	✓	✓				
Khatti and Grover [20]	✓	✓ (deep learning vs traditional)	✓ (performance analysis depth)			
Wang et al. [8]	✓			✓ (Computational variability handling)		
Khan et al. [21]	✓	✓ (ANN, LR, MLR, NLR)	✓ (Sensitivity analysis)			
Mohammed et al. [22]	✓	✓ (ANN, DNN, SVR, RF, XGBoost)	✓ (Explainable AI)			
Adamolekun et al. [23]	✓	✓ (ANN, RF, SVM, XGBoost)	✓ (Feature importance)			
This Study (2025)	✓	✓ (ReLU, Sigmoid, Tanh, Swish)	✓ Coverage Analysis	✓	✓	✓ (Coverage points)

Numerous studies have explored soil compaction prediction using machine learning techniques. Othman and Abdelwahab [3] and Khatti and Grover [16-20] applied models such as ANN, LSSVM, LSTM, and other soft computing approaches to estimate compaction parameters, demonstrating improved predictive accuracy over traditional methods. Comparative analyses of different models have been a common focus in recent works. Khan et al. [21], Mohammed et al. [22], and Khatti and Grover [17, 20] evaluated a range of algorithms, including ANN, DNN, SVR, RF, and XGBoost, to identify optimal predictive frameworks. Efforts to enhance interpretability through Explainable AI (XAI) and sensitivity analysis were highlighted in studies by Mohammed et al. [22] and Adamolekun et al. [23], who assessed feature importance to support model transparency and decision-making. Gurtug et al. [7] and Wang et al. [8] addressed standard line creation and compaction curve variability using statistical prediction and computational

strategies, marking early efforts to integrate standardization into soil compaction studies. Despite advancements in ML applications, geometric algorithms such as Ray-Casting remain largely unexplored in this context, presenting a gap for future innovation in soil behavior modeling. Few studies have proposed new indicators or evaluation metrics specific to standard compaction line accuracy or model validation, signaling a need for more comprehensive and domain-specific performance evaluation frameworks. However, no existing studies combine ML prediction, standard line generation, geometric evaluation, and the development of a new performance indicator, which this study aims to address to enhance accuracy, reliability, and standardization in soil compaction testing, as summarized in Table 1.

This paper aims to apply Artificial Neural Networks (ANN) for predicting soil compaction parameters based on data from Modified Proctor Tests, thereby improving the accuracy and efficiency of assessing compaction characteristics. It also compares the performance of the ANN model using a newly proposed indicator, the coverage points, to evaluate prediction accuracy. Additionally, the study incorporates Explainable AI (XAI) and sensitivity analysis to ensure that the model's predictions align with geotechnical principles and enhance interpretability. A key objective is the development of a standard compaction line derived from Modified Proctor Test parameters using ANN, moving beyond traditional statistical methods. Moreover, the paper introduces a geometric algorithm based on the Ray-Casting technique to construct a coverage area based on tolerance percentages, which is then used to calculate the coverage points. Finally, the study proposes this new indicator and evaluation method as a novel approach to improve the standardization and accuracy of soil compaction testing in geotechnical engineering, offering an alternative to conventional performance metrics.

2. Methodology

2.1 Notation and abbreviation

This section provides definitions of key notations and abbreviations used throughout the study for clarity and consistency as Table 2.

Table 2 The summary of Notation and Abbreviation

Notation / Abbreviation	Definition	Notation / Abbreviation	Definition
OMC	Optimum Moisture Content	RMSE	Root Mean Square Error
MDD	Maximum Dry Density	MAE	Mean Absolute Error
MC	Moisture Content	WMAPE	Weighted Mean Absolute Percentage Error
DD	Dry Density	MAPE	Mean Absolute Percentage Error
GW	Well-Graded Gravel	PI	Performance Index
AASHTO	Soil classification system used in highway engineering	RSR	Ratio of Standard Deviation of Residuals to Standard Deviation of Observations
USCS	Unified Soil Classification System	NS	Nash-Sutcliffe Efficiency
ASTM	American Society for Testing and Materials	VAF	Variance Accounted For
ICC	Intraclass Correlation Coefficient	y_i	Actual value
ANN	Artificial Neural Network	$\hat{y}$	Predicted value
ReLU	Rectified Linear Unit	$\bar{y}$	Mean of actual values
Tanh	Hyperbolic Tangent	N	Number of observations
SL	Standard line	$var(y-\hat{y})$	Variance of the prediction errors
$DD_{upper,i}$	Dry Density value at point i on the standard line	$var(y)$	Variance of the actual values
$DD_{SL,i}$	Upper Dry Density	AVG	Average
$DD_{lower,i}$	Lower Dry Density	SD	Standard Deviation
ε	Tolerance value		

2.2 Soil compaction data and experiment

The soil used in this study is classified as GW under the USCS and as A-2-5 (Clayey Gravel) under the AASHTO classification system. Physically, it is well-graded gravel with a minor silt content. The classifications from both systems align consistently, indicating its suitability as a subbase material for highway construction in accordance with government standards. In terms of basic soil properties, the liquid limit is 49.16, the plasticity index is 3.89, and the specific gravity ranges from 2.65 to 2.70. Figure 2 illustrates the grain size distribution curve for the soil studied.

In the experimental procedure, the soil was sieved through a No. 4 (4.75 mm) sieve, and the moisture content was adjusted incrementally before compaction. The compaction process used a cylindrical mold, with the soil compacted in three layers by a 4.54 kg hammer dropped from a height of 457 mm, as specified by ASTM D1557. This systematic approach ensured consistent and reliable results across all test sets.

The soil compaction experiments in this study followed the Modified Proctor Compaction Test (ASTM D1557) to determine the MDD and OMC under high-energy compaction conditions, which use higher compactive effort compared to the Standard Proctor Test (ASTM D698) [24]. The experiments involved a total of 120 test sets (Figure 1), with each test repeated five times using varying moisture contents of 2%, 4%, 6%, 8%, and 10%. Three operator groups conducted the experiments, with each group performing 30 test sets. The raw data is presented in the appendix, ensuring a comprehensive analysis. Moreover, based on the uncontrollable or variable factors for soil specimens, including inconsistent compaction, uneven hammer strikes, uneven moisture distribution, weighing errors, mould wear, operator skill variation, temperature fluctuations, drying time differences, moisture evaporation, organic material interference, and weighing equipment accuracy, the data were tested for reliability analysis, as shown in Table 3. The results indicate that both DD (0.7799) and MC (0.8604) exhibit good consistency based on the Intraclass Correlation Coefficient (ICC) values, which fall within the range of 0.75 to 0.9. The ICC values reflect the level of agreement or reliability in the measurements, with values above 0.75 indicating a strong degree of consistency. In addition, both the dry density and moisture content datasets were plotted using Bland–Altman plots with confidence intervals to visually show the agreement between repeated measurements, as shown in Figure 3.

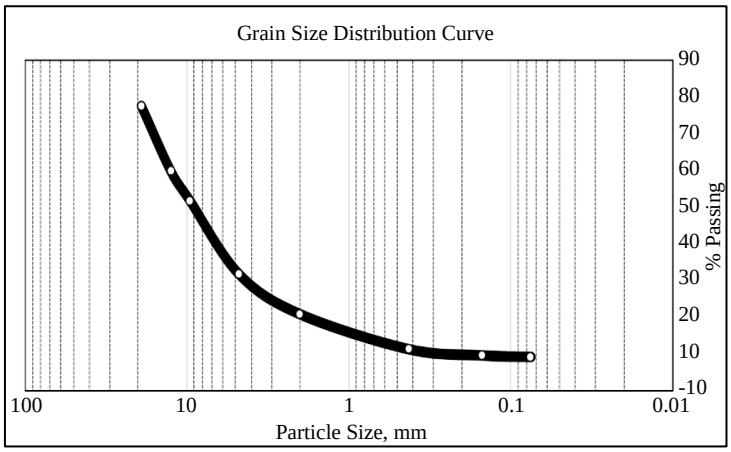

Figure 2 Grain Size Distribution Curve

Table 3 The results of reliable analysis using ICC (One-Way Random Model: (ICC(1))

Dataset	ICC(1)	Consistency
DD	0.7799	Good
MC	0.8604	Good

When ICC < 0.5 (Poor consistency), 0.5 ≤ ICC < 0.75 (Moderate consistency), 0.75 ≤ ICC < 0.9 (Good consistency) and ICC ≥ 0.9 (Excellent consistency)

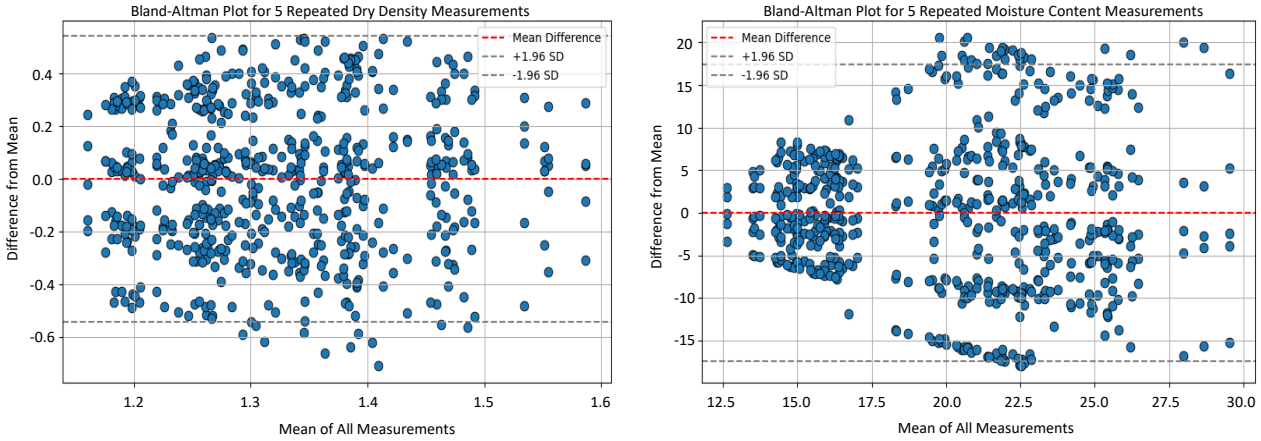

(a) (b)

Figure 3 ICC plots using Bland–Altman plot with confidence intervals, (a) Dry Density, (b) Moisture Content

2.3 Artificial Neural Network (ANN) architecture and activation functions

ANNs have emerged as a robust computational tool for modeling nonlinear relationships in complex datasets. The architecture of an ANN typically consists of an input layer, one or more hidden layers, and an output layer. Each layer is composed of neurons, and the activation function in each neuron determines the output by introducing nonlinearity into the model [25, 26]. Choosing appropriate activation functions is critical for enhancing the learning ability and performance of the ANN [27, 28].

This study incorporates four activation functions—ReLU, Sigmoid, Tanh, and Swish—due to their unique characteristics and suitability for specific applications in modeling soil compaction data. These functions were chosen because they address key challenges such as nonlinearity, vanishing gradients, and model interpretability in the context of predicting standard lines for compaction testing [10, 12, 27].

2.4 Configuration analysis

The sensitivity analysis in this study evaluated the impact of key configurations on the performance of the ANN model, focusing on the number of hidden layers (3, 4, and 5) and the number of dense units (32, 64, and 128). These parameters were systematically varied to assess their influence on the model's ability to predict the optimal standard curve line for soil compaction. To ensure the analysis focused solely on these variables, other configurations were held constant, including a test size of 0.2, a random state of 45 for reproducibility, 1000 epochs, a batch size of 10, and a validation split of 0.2. This approach provided a controlled environment to isolate the effects of the number of hidden layers and dense units, offering valuable insights into optimizing the ANN model for reliable and accurate soil compaction predictions. The summary is shown in Table 4.

Table 4 Summary of Configuration

Configuration	Test size	Random state	Epochs	Batch size	Validation split	Hidden layers	Dense units
1						3	32
2						3	64
3						3	128
4						4	32
5	0.2	45	1000	10	0.2	4	64
6						4	128
7						5	32
8						5	64
9						5	128

Moreover, the model is configured with the Adam optimizer and a mean squared error (MSE) loss function. Adam is a popular optimization algorithm known for its efficiency and adaptive learning rate, making it well-suited for training deep learning models. The choice of MSE as the loss function is commonly used for regression tasks, as it penalizes large deviations between predicted and actual values, helping the model learn to minimize the error in predictions effectively.

2.5 Coverage area analysis and ray-casting algorithm

The coverage area analysis was conducted to evaluate how well the standard line (SL) represents the compaction data by determining the number of data points that fall within a defined tolerance region around it, as shown in Figure 4. The tolerance region was defined by two boundaries, represented by two equations. The upper boundary for each data point i was calculated as $DD_{upper,i} = DD_{SL,i} + \varepsilon$ where $DD_{SL,i}$ is the Dry Density value at point i on the standard line, and ε is the tolerance value. The lower boundary for each data point i was calculated as $DD_{lower,i} = DD_{SL,i} - \varepsilon$

Moreover, to determine whether each data point falls within this coverage area as the coverage points, the Ray-Casting Algorithm was employed. This algorithm works by casting a horizontal ray from the data point and counting the number of intersections it makes with the polygon's edges. If the number of intersections is odd, the point is classified as being inside the polygon; if even, it is classified as outside. The steps of the algorithm involve iterating through all edges of the polygon, checking for ray-edge intersections, and toggling the classification based on the number of intersections. The area between these boundaries forms a polygonal region around the standard line that represents the allowable deviation for DD across the specified range of data, as shown in Figure 5.

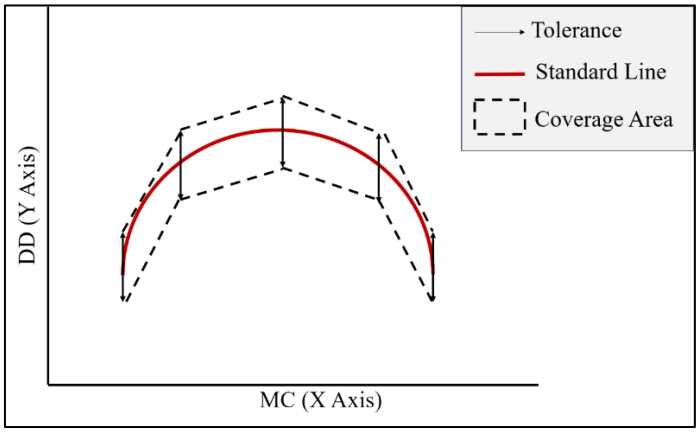

Figure 4 Coverage area From Standard ± Tolerance

```python
def is_point_in_polygon(point, polygon):
    x, y = point
    n = len(polygon)
    inside = False
    px, py = polygon[-1]
    for i in range(n):
        sx, sy = polygon[i]
        if ((sy >= y) != (py >= y)) and (x < (px - sx) * (y - sy) / (py - sy) + sx):
            inside = not inside
        px, py = sx, sy
    return inside
```

Figure 5 Ray-Casting Algorithm in Python

Moreover, while the study accounts for variations in DD by applying a tolerance band, the MC is treated as constant and represented by its average value across the dataset. This approach simplifies the analysis, focusing on the variability in DD while maintaining a consistent reference for MC. By combining these methods, the study evaluates the coverage area and quantifies the number of data points included within the tolerance-defined region using the Ray-Casting Algorithm.

2.6 Tolerance scenario

To evaluate the performance of the standard line in representing soil compaction data, three tolerance scenarios—2%, 5%, and 10%—were applied. The 5% tolerance level was selected based on recommendations from the Civil Engineering and Development Department (CEDD) of Hong Kong, which uses this threshold as a standard in soil compaction assessments. The 2% and 10% scenarios were included to analyze the effects of selecting tolerances that are either too low or too high. A 2% tolerance represents a strict scenario, capturing minimal deviations from the standard line, which may exclude valid data points and lead to overly restrictive evaluations. Conversely, a 10% tolerance represents a lenient scenario, allowing for broader deviations, which may compromise the reliability of the standard line by overestimating the acceptable range. These varying tolerance levels directly impact the number of data points covered within the defined coverage area, with lower tolerances reducing the number of covered points and higher tolerances increasing it. By comparing these three scenarios, this study aims to understand how tolerance levels influence the number of points within the coverage area and, consequently, the accuracy and applicability of the standard line in compaction testing.

2.7 Performance evaluation

The regular performance metrics of an ANN model were evaluated using four activation functions—ReLU, Sigmoid, Tanh, and Swish—across nine configurations (1 to 9), based on multiple indicators. RMSE, as shown in Equation 1, and MAE, as shown in Equation 2, measure the magnitude of prediction errors, with lower values indicating better performance [29, 30]. WMAPE, as shown in Equation 3, and MAPE, as shown in Equation 4, express prediction errors in relation to actual values, where lower values are preferable [31, 32]. PI, as shown in Equation 5, assesses model effectiveness, with higher values indicating better performance [33]. RSR, as shown in Equation 6, should be minimized for improved accuracy [34]. NS, as shown in Equation 7, ranges from negative values to 1 and is optimal when closer to 1, representing higher predictive power [35]. VAF, as shown in Equation 8, measures model fit, with higher values suggesting a better match between predicted and actual outcomes [36].

$$\mathrm{RMSE} = \sqrt{\frac{1}{n}\sum_{i=1}^{n}(y_i - \hat{y}_i)^2} \tag{1}$$

$$\mathrm{MAE} = \frac{1}{n}\sum_{i=1}^{n}|y_i - \hat{y}_i| \tag{2}$$

$$\mathrm{WMAPE} = \sum_{i=1}^{n}\frac{\sum_{i=1}^{n}|y_i - \hat{y}_i|}{\sum_{i=1}^{n} y_i} \tag{3}$$

$$\mathrm{MAPE} = \frac{100\%}{n}\sum_{i=1}^{n}\left|\frac{y_i - \hat{y}_i}{y_i}\right| \tag{4}$$

$$\mathrm{PI} = \frac{1}{n}\sum_{i=1}^{n}\left(1 - \frac{|y_i - \hat{y}_i|}{y_i}\right) \times 100 \tag{5}$$

$$\mathrm{RSR} = \frac{\mathrm{RMSE}}{\sqrt{\frac{1}{n}\sum_{i=1}^{n}(y_i - \bar{y})^2}} \tag{6}$$

$$\mathrm{NS} = 1 - \frac{\sum_{i=1}^{n}(y_i - \hat{y}_i)^2}{\sum_{i=1}^{n}(y_i - \bar{y})^2} \tag{7}$$

$$\mathrm{VAF} = \left[1 - \frac{\mathrm{var}(y - \hat{y})}{\mathrm{var}(y)}\right] \times 100\% \tag{8}$$

3. Results

3.1 Comparison of compaction curves using different activation functions

The performance of the ANN was evaluated by examining the compaction curves generated using different activation functions: ReLU, Sigmoid, Tanh, and Swish. The compaction curves, represented by DD versus MC, were analyzed across nine configurations to assess the behavior of each activation function in modeling the standard line.

The compaction curves produced using the ReLU activation function (Figure 6a) exhibit a well-defined peak corresponding to the MD at the OMC. The results indicate that ReLU effectively captures the nonlinear relationship between DD and MC, maintaining consistent patterns across all configurations. The sharp transitions in the curves highlight the capability of ReLU to handle abrupt changes in data, making it suitable for modeling compaction characteristics.

In contrast, the Sigmoid activation function (Figure 6b) displays flatter and less dynamic compaction curves. The results reveal that Sigmoid struggles to capture the peak MDD and OMC accurately, particularly in higher configurations. This limitation can be

attributed to the vanishing gradient problem associated with the Sigmoid function, which leads to reduced sensitivity to changes in the input data. Consequently, the compaction curves show minimal variation across configurations, indicating suboptimal performance in representing the standard line.

The Tanh activation function (Figure 6c) produces compaction curves with clear peaks, similar to ReLU. The results demonstrate that Tanh effectively captures the nonlinear relationship between DD and MC, with smoother transitions than ReLU. However, some configurations exhibit steeper gradients, indicating a more aggressive response to changes in MC. This makes Tanh a robust choice for modeling compaction data while maintaining sensitivity to input variability.

The Swish activation function (Figure 6d) generates compaction curves that combine the strengths of ReLU and Tanh. The curves display well-defined peaks and smooth transitions, highlighting the effectiveness of Swish in modeling the standard line. The results suggest that Swish maintains a balanced response to input changes, avoiding the vanishing gradient issue of Sigmoid while capturing the nonlinear behavior effectively. Its performance is consistent across all configurations, making it a promising activation function for this application.

The comparative analysis of the four activation functions indicates that ReLU, Tanh, and Swish perform well in modeling compaction data, with Swish providing the most balanced and consistent results. Sigmoid, however, underperforms due to its inherent limitations in handling complex nonlinear relationships. This evaluation provides valuable insights into selecting the most suitable activation function for predicting compaction characteristics using ANN.

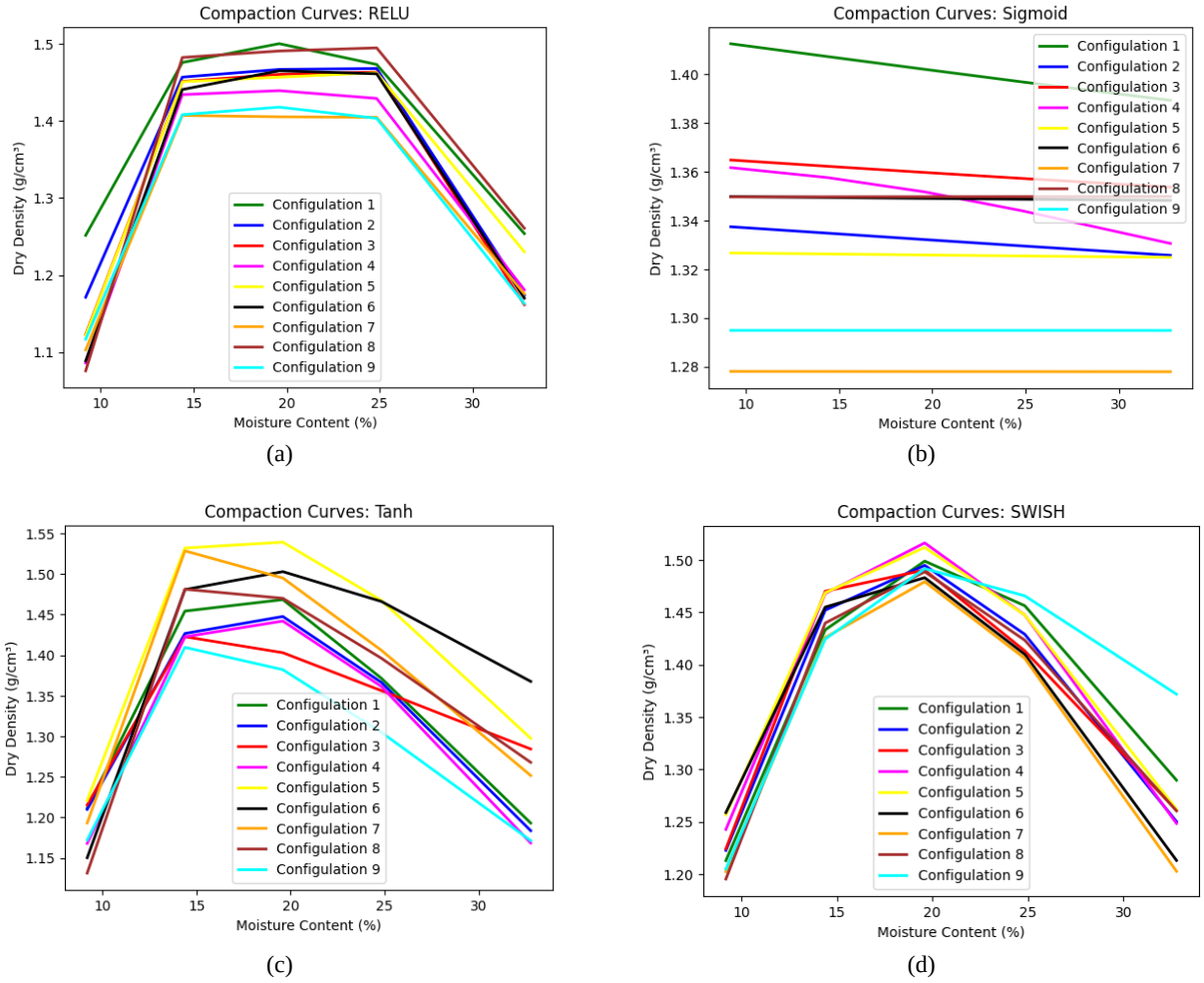

Figure 6 Compaction curve prediction, (a) RELU, (b) Sigmoid, (c) Tanh, (d) Swish,

3.2 Coverage analysis of compaction data across tolerance levels

The evaluation of compaction curves was extended to analyze the coverage area using three tolerance levels: 2%, 5%, and 10%. The number of DD spots covered by the standard line under each tolerance scenario was calculated, with higher coverage indicating the method's effectiveness in capturing the variability within the compaction data. Below is a detailed analysis of each tolerance level, supported by bar charts and boundary coverage figures.

The 2% tolerance level resulted in the lowest number of DD spots across all configurations and activation functions (Figure 7). The strict tolerance tightly constrained the boundaries, leading to overfitting and multiple overlapping peaks in the coverage areas. The average method (Figure 8a) highlighted the limitations of a fixed approach, producing narrow boundaries and failing to generalize effectively. Swish performed relatively well, particularly Swish1 and Swish4 (Figures 8b and 8c), compared to ReLU and Tanh. However, Sigmoid consistently underperformed, capturing fewer DD spots. ReLU1 and ReLU2 (Figures 8d and 8e) showed slightly better performance, while Tanh5 and Tanh7 (Figures 8f and 8g) captured some variability but still exhibited multiple peaks. Overall, the 2% tolerance was too restrictive, resulting in poor generalization and reduced model accuracy.

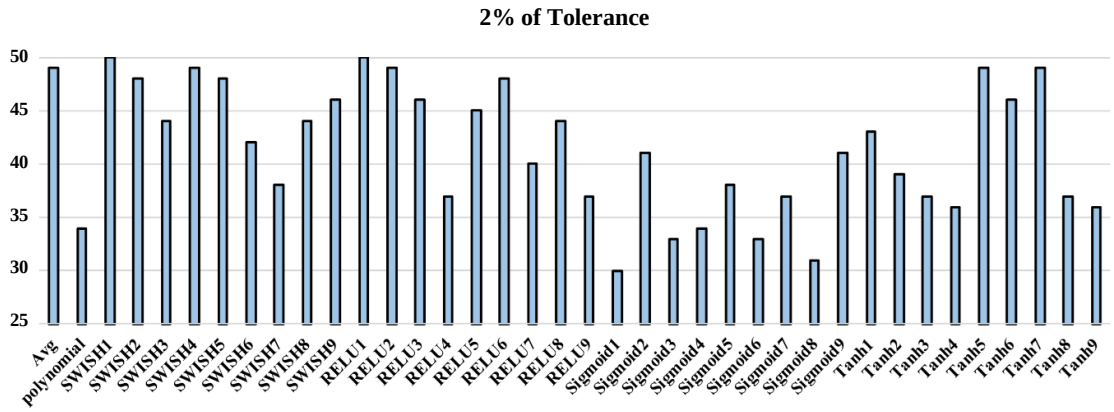

Figure 7 Coverage points at 2% of tolerance

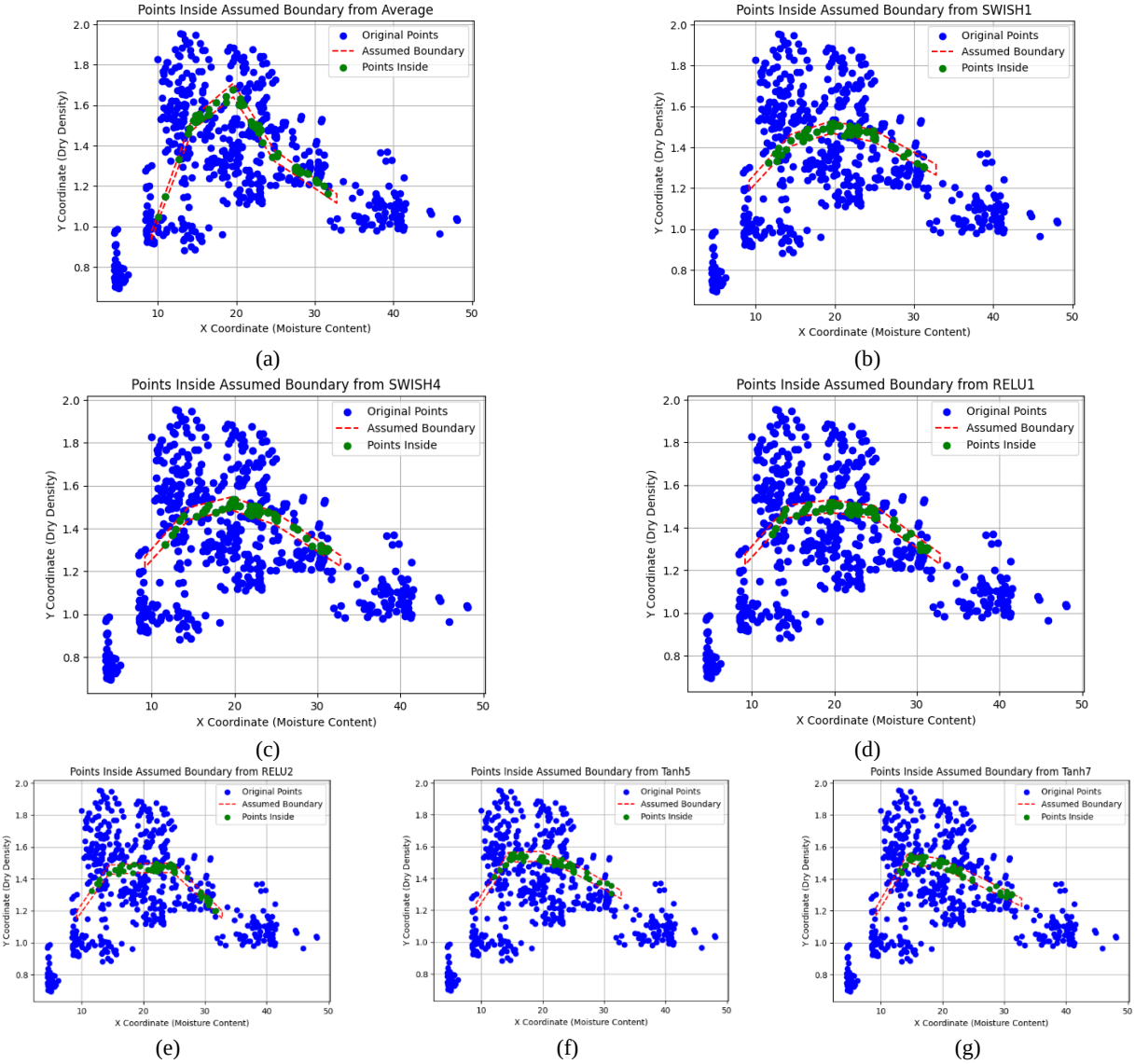

Figure 8 Comparison the peak from 2% tolerance result among, (a) Average, (b) SWISH1, (c) SWISH4, (d) RELU1, (e) RELU2, (f) Tanh5, (g) Tanh7

The 5% tolerance level, as shown in the bar chart (Figure 9), exhibited a balanced increase in DD spots covered across all configurations. This level is considered optimal, balancing strictness and coverage. Swish6 achieved the highest coverage (Figure 10a), capturing the single peak corresponding to the MDD at the OMC. The boundary effectively modeled the compaction curve, maintaining high sensitivity to the data's nonlinear behavior. In contrast, Sigmoid1 showed the lowest coverage (Figure 10b), with flatter boundaries that failed to represent the MDD accurately. The comparative figures demonstrate Swish6's ability to model the curve effectively, while Sigmoid1 struggled to capture critical features.

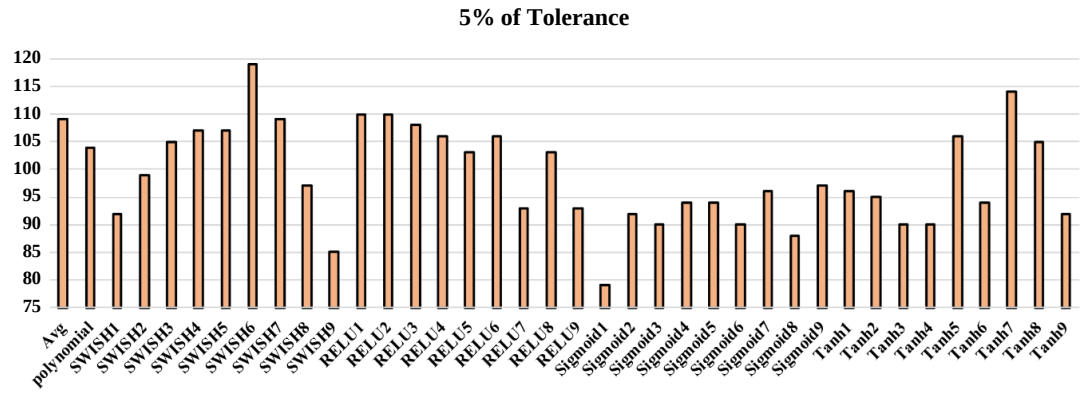

Figure 9 Coverage points at 5% of tolerance

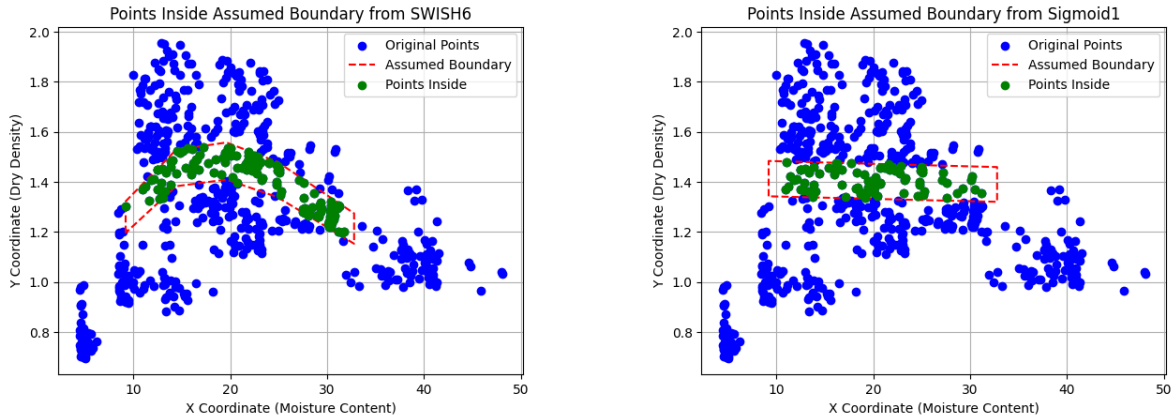

(a) (b)

Figure 10 Comparison the highest and the lowest from 5% tolerance result between, (a) SWISH6, (b) Signoid1

The 10% tolerance level produced the highest number of DD spots covered, as illustrated in Figure 11. This lenient tolerance allowed for broader deviations, capturing a wider range of compaction data. However, it also introduced errors by overgeneralizing the data representation. Tanh3 (Figure 12a) maintained the expected curve shape, accurately capturing the MDD, while Sigmoid1 (Figure 12b) displayed a nearly rectangular boundary that failed to reflect the nonlinear compaction behavior. The figures highlight the trade-off at this level: while higher tolerances increase coverage, they compromise accuracy by overgeneralizing the coverage area, particularly for models like Sigmoid.

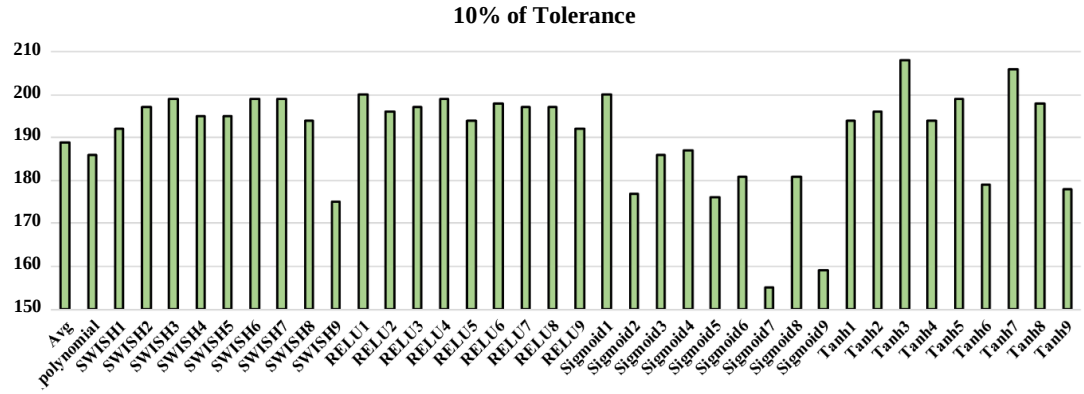

Figure 11 Coverage points at 10% of tolerance

The comparative analysis across tolerance levels revealed that Swish consistently outperformed other activation functions in terms of coverage, regardless of the tolerance. ReLU and Tanh also delivered strong results, especially under 5% and 10% tolerances, while Sigmoid underperformed due to its inherent limitations. The findings suggest that the 5% tolerance level offers the best balance between strictness and coverage, aligning with practical recommendations for compaction analysis. A 2% tolerance was too restrictive, resulting in multiple overlapping peaks and reduced accuracy, while a 10% tolerance was too lenient, introducing overgeneralization errors. The 5% tolerance emerged as the most reasonable option, providing a balanced representation of the compaction data and allowing for accurate modeling of the MDD and OMC. Swish, ReLU, and Tanh demonstrated strong performance, with Swish achieving the best overall results.

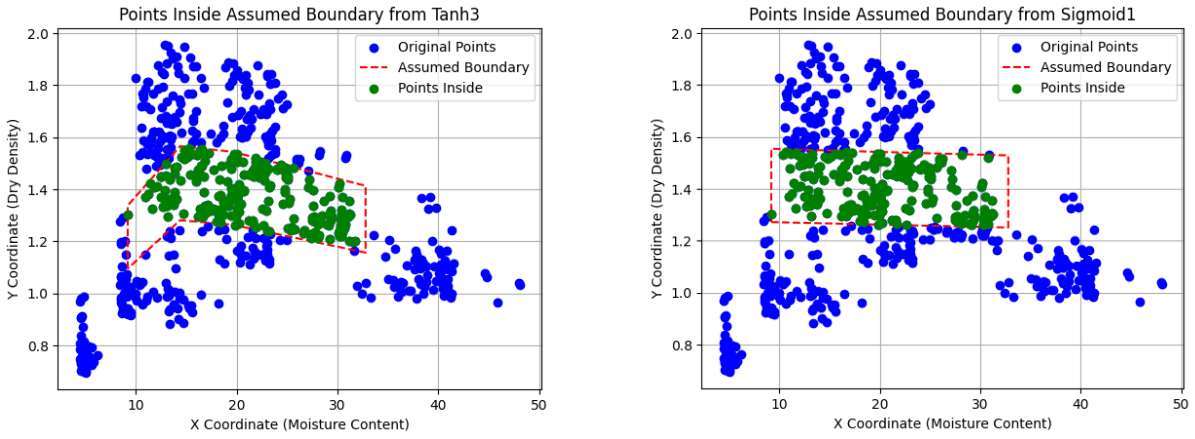

Figure 12 Comparison the peak from 10% tolerance result between, (a) Tanh3, (b) Sigmoid1

In addition, Swish emerged as the most effective model for generating a standard line for compaction testing. Its superior ability to capture the nonlinear relationship between DD and MC ensures that the compaction curve is accurately represented while maintaining high coverage under varying tolerances. These qualities make Swish the ideal activation function for establishing reliable and practical standards for compaction testing, offering precision, adaptability, and robustness across diverse scenarios.

Table 5 Results of regular performance measurements

Activation Functions	Config.	Regular Performance Measurements							
		RMSE (Lowest)	MAE (Lowest)	WMAPE (Lowest)	MAPE (Lowest)	PI (Highest)	RSR (Lowest)	NS (Highest)	VAF (Highest)
Ideal Values		0	0	0	0	100	0	1	100
ReLU	**1**	0.1934	0.1452	11.2299	11.3964	60.8333	0.6449	0.5806	58.2058
	2	0.1915	0.1422	10.9949	11.0462	62.5000	0.6387	0.5887	58.8662
	3	0.1961	0.1423	11.0051	10.6556	59.1667	0.6540	0.5687	58.6992
	4	0.1925	0.1434	11.0843	11.2353	61.6667	0.6418	0.5846	58.5389
	5	0.1946	0.1428	11.0413	11.0634	62.5000	0.6488	0.5755	57.6434
	6	0.1910	0.1407	10.8800	10.9784	64.1667	0.6370	0.5909	59.1227
	7	0.1942	0.1441	11.1432	11.1470	56.6667	0.6478	0.5768	57.8088
	8	0.2005	0.1511	11.6865	11.7390	51.6667	0.6687	0.5490	55.3482
	9	0.1940	0.1437	11.1138	11.2214	65.0000	0.6469	0.5780	57.8206
Sigmoid	**1**	0.2989	0.2444	18.8998	21.3936	34.1667	0.9968	-0.0020	1.0456
	2	0.2982	0.2449	18.9359	21.2040	33.3333	0.9946	0.0025	0.6734
	3	0.3015	0.2452	18.9614	21.7158	34.1667	1.0056	-0.0197	0.5981
	4	0.2995	0.2471	19.1055	21.4010	32.5000	0.9987	-0.0057	0.0580
	5	0.2957	0.2412	18.6492	20.5824	33.3333	0.9863	0.0191	1.9414
	6	0.3003	0.2463	19.0429	21.5484	34.1667	1.0015	-0.0114	0.2077
	7	0.3007	0.2478	19.1632	21.6294	31.6667	1.0027	-0.0139	-0.0027
	8	0.3073	0.2512	19.4213	22.4933	30.8333	1.0248	-0.0591	0.0150
	9	0.2988	0.2481	19.1817	20.8916	32.5000	0.9965	-0.0014	0.0064
Tanh	**1**	0.2171	0.1737	13.4294	13.7667	44.1667	0.7240	0.4714	47.1652
	2	0.2118	0.1711	13.2295	13.7324	44.1667	0.7063	0.4970	50.2719
	3	0.2225	0.1819	14.0617	14.5970	40.0000	0.7421	0.4446	46.9425
	4	0.2099	0.1639	12.6739	13.2412	47.5000	0.6999	0.5061	50.6213
	5	0.2014	0.1528	11.8120	11.9442	50.8333	0.6718	0.5449	54.7848
	6	0.2171	0.1689	13.0623	12.7692	49.1667	0.7240	0.4714	54.6921
	7	0.2121	0.1646	12.7271	13.8099	50.0000	0.7074	0.4954	50.2030
	8	0.2019	0.1592	12.3088	12.9965	48.3333	0.6735	0.5426	56.5586
	9	0.2093	0.1687	13.0436	13.5280	47.5000	0.6980	0.5087	52.9026
Swish	**1**	0.2072	0.1620	12.5220	12.7061	49.1667	0.6908	0.5187	51.8785
	2	0.2035	0.1574	12.1708	12.7326	52.5000	0.6786	0.5356	54.0790
	3	0.2067	0.1655	12.7973	13.2418	45.8333	0.6892	0.5210	53.4562
	4	0.2062	0.1614	12.4802	12.8740	50.0000	0.6878	0.5230	52.3308
	5	0.2123	0.1687	13.0454	14.0815	50.8333	0.7079	0.4947	51.0623
	6	0.2042	0.1561	12.0712	12.5091	50.8333	0.6810	0.5323	53.2408
	7	0.2100	0.1667	12.8911	13.5991	51.6667	0.7004	0.5053	50.8801
	8	0.2035	0.1556	12.0278	11.9762	50.8333	0.6786	0.5356	53.7964
	9	0.2053	0.1582	12.2352	12.6837	51.6667	0.6847	0.5273	52.7333
Best Value		0.1910	0.1407	10.8800	10.6556	65.0000	0.6370	0.5909	59.1227
Best Activation Function		ReLU	ReLU	ReLU	ReLU	ReLU	ReLU	ReLU	ReLU

3.3 Performance measurement results

As shown in Table 5, the evaluation of activation functions in the ANN model highlights distinct performance trends. ReLU performed well, with Config 6 (RMSE: 0.1910, MAE: 0.1407) and Config 2 (RMSE: 0.1915, MAE: 0.1422) showing the lowest errors, along with strong WMAPE and MAPE values. The highest Performance Index (PI) of 65.0000 appeared in Config 9, while VAF ranged from 55.3482 to 59.1227, indicating reasonable variance explanation. Sigmoid performed the worst, with significantly higher RMSE and MAE across all configurations, and the best NS value of only 0.0191 (Config 5), indicating poor predictive power, while VAF values remained near zero. Tanh performed better than Sigmoid but slightly worse than ReLU and Swish, with Config 5 (RMSE: 0.2014, MAE: 0.1528, VAF: 54.7848) and Config 8 (RMSE: 0.2019, MAE: 0.1592, VAF: 56.5586) showing the best results. PI values

for Tanh ranged from 40.0000 to 50.8333, reflecting moderate performance. Swish emerged as one of the best activation functions overall, with Config 2 (RMSE: 0.2035, MAE: 0.1574, VAF: 54.0790) and Config 8 (RMSE: 0.2035, MAE: 0.1556, VAF: 53.7964) demonstrating optimal performance. The best RSR value of 0.6786 (Configs 2 and 8) signaled superior model stability, while NS values were consistently higher than those of Tanh and significantly better than Sigmoid.

However, the best-performing activation function across all regular performance metrics was ReLU, demonstrating the lowest errors and highest predictive accuracy. Config 6 achieved the best results for RMSE (0.1910), MAE (0.1407), WMAPE (10.8800), RSR (0.6370), NS (0.5909), and VAF (59.1227), making it the most effective configuration overall. Config 3 provided the lowest MAPE (10.6556), while Config 9 achieved the highest PI of 65.0000, further confirming ReLU's superiority in this ANN model evaluation. This demonstrates that the proposed method, Coverage Analysis of Compaction Data Across Tolerance Levels, yields different performance measurements compared to those that produce the same results as ReLU.

4. Discussion

This study significantly advances the field of soil compaction testing by addressing key gaps identified in prior research and providing novel contributions to the modeling of standard lines for compaction curves. Traditional studies, such as those by [6] and [7], focused on statistical and mean-based methods for generating standard lines. These approaches, while foundational, lacked the capacity to adapt to nonlinear data and failed to capture variability effectively, particularly in complex soil compositions, as highlighted by [3]. This study bridges this gap by leveraging Artificial Neural Networks (ANNs) to model compaction data dynamically, enabling the generation of standard lines that account for nonlinear relationships. Moreover, while previous works like [8] and [9] emphasized the challenges posed by environmental conditions and operator-induced errors in compaction testing, this study incorporates a robust tolerance-based evaluation framework to mitigate these issues. By applying tolerance levels (2%, 5%, and 10%) to analyze coverage areas, this research introduces a performance evaluation metric grounded in geometric algorithms, building on prior geometric methods explored by [1] and [6]. The use of the Ray-Casting Algorithm to determine the inclusion of data points within tolerance boundaries represents a novel approach in soil mechanics, as suggested by [13] and [23].

This study also diverges from earlier research, such as [6] and [7], which primarily focused on unifying compaction curves through computational techniques but did not provide a clear evaluation metric for standard line performance. By integrating Swish, ReLU, Tanh, and Sigmoid activation functions, this research aligns with recent advancements in machine learning, including studies by [24] and [28]. The comparative analysis across activation functions revealed that Swish consistently outperformed the others, providing the most accurate and adaptable standard line for compaction testing, further validating findings by [26] and [27] on the effectiveness of Swish in capturing nonlinear patterns.

This study shows that the Swish activation-based ANN model outperforms the ReLU, Sigmoid, and Tanh-based ANN models in the context of compaction data characteristics. Swish is a smooth and non-monotonic activation function, which enables the model to learn more complex and subtle nonlinear relationships between input variables, such as Dry Density (DD) and Moisture Content (MC) [24, 27]. This is essential for modeling compaction curves, which do not follow simple linear or monotonic patterns. Moreover, Swish supports self-gating, meaning the function adjusts its own output based on the input, providing adaptive flexibility during learning [27]. This leads to more precise curve fitting and better generalization when handling real-world variations in soil compaction behavior. Furthermore, the gradient flow in Swish remains active across both positive and negative input ranges, avoiding gradient vanishing or dead neuron problems that can hinder training with other functions [24, 26, 28]. As a result, networks trained with Swish converge more efficiently and reliably, especially in deeper architectures or more variable datasets [25, 27]. Finally, Swish inherently balances the benefits of both linear and nonlinear activation, allowing it to remain sensitive to small input changes while also promoting robust learning across broader input domains [27, 28]. These properties make Swish particularly well-suited for establishing standard lines in compaction testing, where accurate curve modeling under varying tolerances is critical.

Furthermore, tolerance-based evaluations were enhanced by applying tolerance levels to optimize performance, an approach inspired by [34]. This allowed for a balanced analysis that aligns with practical recommendations while addressing the shortcomings of overly strict or lenient tolerance levels, as previously identified by [31]. The study's emphasis on the 5% tolerance level, supported by geometric evaluations, ensures a reliable framework for compaction testing that surpasses traditional methods, as explored by [1] and [6].

In addition to contributing new methodological insights, this study expands on the application of computational models in soil mechanics. Unlike prior studies such as [10] and [3], which focused on basic ANN implementations, this research incorporates multiple activation functions and evaluates their impact on tolerance-based coverage. This approach closes the gap in understanding how activation functions influence the generalizability of standard lines, building on the work by [24] and [28].

Artificial Neural Networks (ANNs) are highly effective in predicting soil compaction parameters such as Maximum Dry Density (MDD) and Optimum Moisture Content (OMC) due to their ability to model complex, non-linear relationships, particularly in large datasets with varied input features [3, 10, 15]. However, ANNs can require more computational resources and longer training times compared to other machine learning techniques. Support Vector Machines (SVMs) tend to offer high accuracy, especially for smaller, well-structured datasets, but may struggle with larger or noisier datasets unless kernel adjustments are made [17]. Random Forests (RF), being an ensemble method, are robust to noisy data and computationally less demanding than ANNs, although they might not capture highly complex, non-linear relationships as effectively [17, 21]. k-Nearest Neighbors (k-NN), while simple and intuitive, may encounter challenges with large datasets due to high computational costs during prediction and performance degradation in high-dimensional spaces [11]. Gradient Boosting (GB) often excels in precision for non-linear relationships but is more computationally expensive and can be prone to overfitting without proper tuning [21, 22]. Ultimately, the selection of a model depends on the dataset size, complexity, and available computational resources.

In conclusion, this study closes several gaps in soil compaction research by introducing machine learning-driven methodologies, tolerance-based performance metrics, and geometric algorithms for coverage evaluation. It establishes Swish as the optimal activation function for generating standard lines, outperforming traditional statistical and computational methods. By addressing variability, operator-induced errors, and nonlinear data patterns, this research lays the groundwork for more accurate, adaptable, and reliable standards in soil compaction testing.

5. Conclusion

This study has significantly advanced the modeling of standard lines for soil compaction testing by introducing Artificial Neural Networks (ANNs) and tolerance-based evaluation metrics. By addressing key gaps in traditional methodologies, such as mean-based and polynomial fitting approaches, the research demonstrates the potential of machine learning to handle nonlinear relationships and dataset variability more effectively. The integration of Swish, ReLU, Tanh, and Sigmoid activation functions into ANN models provided a comprehensive comparison, with Swish emerging as the most effective activation function for generating accurate and reliable standard lines. The use of a robust geometric algorithm, the Ray-Casting Algorithm, allowed for precise evaluation of coverage areas, accounting for variability within the dataset. Tolerance levels of 2%, 5%, and 10% were analyzed, with the 5% tolerance level identified as the most balanced approach, offering reliable standard lines while minimizing overfitting or overgeneralization. This research contributes significantly to geotechnical engineering by introducing a machine learning-driven framework that enhances the accuracy, adaptability, and standardization of compaction testing.

The use of Artificial Neural Networks (ANNs) for predicting Modified Proctor Test results faces several limitations. One of the main challenges is handling highly variable data, such as uneven moisture content in soil samples and environmental fluctuations, which can lead to decreased model accuracy. Additionally, the complexity of ANN models makes it difficult to interpret their results, which can reduce the reliability of the findings. The process of selecting appropriate model parameters, such as the number of layers or neurons, requires extensive testing and tuning, which may lead to instability in the results. These factors hinder the overall performance and reliability of ANN models in the context of soil compaction testing.

Future research should focus on addressing these limitations and enhancing the applicability of ANN models for Modified Proctor Test predictions. Studies could validate the framework across diverse soil types, incorporate environmental factors such as temperature and humidity, and develop hybrid models combining ANNs with advanced techniques like Support Vector Machines (SVM) or Random Forests to improve accuracy and reduce overfitting. Real-time applications using IoT devices for environmental monitoring, optimization of activation functions, and exploration of alternative geometric algorithms could further strengthen model reliability and precision. Additionally, integrating other geotechnical tests, such as permeability and consolidation, would expand the model's practical use. Importantly, applying explainable AI (XAI) techniques, such as SHAP or LIME, would improve the interpretability of ANN results, enhance model transparency, and support practical decision-making. Finally, developing performance indicators specifically tailored to compaction data analysis would improve the evaluation of standard lines and coverage accuracy.

6. References

[1] Almuaythir S, Zaini MSI, Lodhi RH. Predicting soil compaction parameters in expansive soils using advanced machine learning models: a comparative study. Sci Rep. 2025;15(1):24018.
[2] ASTM. ASTM D698-12e2: standard test methods for laboratory compaction characteristics of soil using standard effort. West Conshohocken: ASTM International; 2012.
[3] Othman K, Abdelwahab H. Prediction of the soil compaction parameters using deep neural networks. Transp Infrastruct Geotech. 2023;10:147-64.
[4] Jalal FE, Xu Y, Iqbal M, Jamhiri B, Javed MF. Predicting the compaction characteristics of expansive soils using two genetic programming-based algorithms. Transp Geotech. 2021;30:100608.
[5] Okonkwo UN, Ekeoma EC, Eleke LO. Polynomial models for predicting time limits for compaction after mixing operation of lateritic soil reinforced using cement or lime. J Civ Eng Sci Technol. 2023;14(1):26-34.
[6] Zainal AKE. Mathematical modeling of compaction curve using normal distribution functions. J Eng. 2018;24(2):118-30.
[7] Gurtug Y, Sridharan A, İkizler SB. Simplified method to predict compaction curves and characteristics of soils. Iran J Sci Technol Trans Civ Eng. 2018;42(6):207-16.
[8] Wang X, Li J, Li J, Zhang J, Ma G. Advanced intelligent compaction strategy for subgrade soil considering heterogeneous database. J Rock Mech Geotech Eng. 2025;17(5):3265-79.
[9] Yao Y, Song E. Intelligent compaction methods and quality control. Smart Constr Sustain Cities. 2023;1:2.
[10] Sinha SK, Wang MC. Artificial neural network prediction models for soil compaction and permeability. Geotech Geol Eng. 2008;26(1):47-64.
[11] Aydın Y, Işıkdağ Ü, Bekdaş G, Nigdeli SM, Geem ZW. Use of machine learning techniques in soil classification. Sustainability. 2023;15(3):2374.
[12] Wang HL, Yin ZY. High performance prediction of soil compaction parameters using multi-expression programming. Eng Geol. 2020;276:105758.
[13] Yaghoubi E, Yaghoubi E, Khamees A, Vakili AH. A systematic review and meta-analysis of artificial neural network, machine learning, deep learning, and ensemble learning approaches in field of geotechnical engineering. Neural Comput Appl. 2024;36:12655-99.
[14] Lee KL, Singh A. Relative density and relative compaction. J Soil Mech Found Div. 1971;97(7):1049-52.
[15] Li B, You Z, Ni K, Wang Y. Prediction of soil compaction parameters using machine learning models. Appl Sci. 2024;14(7):2716.
[16] Khatti J, Grover KS. Determination of the optimum performance AI model and methodology to predict the compaction parameters of soils. ICTACT J Soft Comput. 2022;12(3):2640-50.
[17] Khatti J, Grover KS. Prediction of compaction parameters of compacted soil using LSSVM, LSTM, LSBoostRF, and ANN. Innov Infrastruct Solut. 2023;8(1):76.
[18] Khatti J, Grover KS. Assessment of fine-grained soil compaction parameters using advanced soft computing techniques. Arab J Geosci. 2023;16(3):208.
[19] Khatti J, Grover KS. Evaluation of compactive parameters of soil using machine learning. In: Muthukkumaran K, Ayothiraman R, Kolathayar S, editors. Soil Dynamics, Earthquake and Computational Geotechnical Engineering. Lecture Notes in Civil Engineering, vol 300. Singapore: Springer; 2023. p. 1-14.
[20] Khatti J, Grover KS. Prediction of compaction parameters for fine-grained soil: critical comparison of the deep learning and standalone models. J Rock Mech Geotech Eng. 2023;15(11):3010-38.

[21] Khan MHA, Jafri TH, Ud-Din S, Ullah HS, Nawaz MN. Prediction of soil compaction parameters through the development and experimental validation of Gaussian process regression models. Environ Earth Sci. 2024;83:129.
[22] Mohammed AMA, Husain O, Abdulkareem M, Yunus NZM, Jamaludin N, Mutaz E, et al. Explainable artificial intelligence for predicting the compressive strength of soil and ground granulated blast furnace slag mixtures. Results Eng. 2025;25:103637.
[23] Adamolekun LB, Saliu MA, Lawal AI, Okewale IA. Development of machine learning-based standalone GUI application for predicting hydraulic conductivity and compaction parameters of lateritic soils. Sci Afr. 2024;26:e02393.
[24] Szandała T. Review and comparison of commonly used activation functions for deep neural networks [Internet]. arXiv [Preprint]. 2020 [cited 2025 Apr 2]. Available from: https://arxiv.org/abs/2010.09458.
[25] Goodfellow I, Bengio Y, Courville A. Deep Learning. London: MIT Press; 2016.
[26] Agarap AF. Deep learning using rectified linear units (ReLU) [Internet]. arXiv [Preprint]. 2018 [cited 2025 Jan 15]. Available from: https://arxiv.org/abs/1803.08375.
[27] Ramachandran P, Zoph B, Le QV. Searching for activation functions [Internet]. arXiv [Preprint]. 2017 [cited 2025 Jan 15]. Available from: https://arxiv.org/abs/1710.05941.
[28] Nwankpa C, Ijomah W, Gachagan A, Marshall S. Activation functions: comparison of trends in practice and research for deep learning [Internet]. arXiv [Preprint]. 2018 [cited 2025 Jan 15]. Available from: https://arxiv.org/abs/1811.03378.
[29] Willmott CJ, Matsuura K. Advantages of the mean absolute error (MAE) over the root mean square error (RMSE) in assessing average model performance. Clim Res. 2005;30(1):79-82.
[30] Chai T, Draxler RR. Root mean square error (RMSE) or mean absolute error (MAE)? arguments against avoiding RMSE in the literature. Geosci Model Dev. 2014;7(3):1247-50.
[31] Flores BE. A pragmatic view of accuracy measurement in forecasting. Omega. 1986;14(2):93-8.
[32] de Myttenaere A, Golden B, Le Grand B, Rossi F. Mean absolute percentage error for regression models. Neurocomputing. 2016;192:38-48.
[33] Japkowicz N, Shah M. Performance evaluation in machine learning. In: El Naqa I, Li R, Murphy M, editors. Machine Learning in Radiation Oncology. Cham: Springer; 2015. p. 41-56.
[34] Moriasi DN, Arnold JG, Van Liew MW, Bingner RL, Harmel RD, Veith TL. Model evaluation guidelines for systematic quantification of accuracy in watershed simulations. Trans ASABE. 2007;50(3):885-900.
[35] Nash JE, Sutcliffe JV. River flow forecasting through conceptual models: part I—a discussion of principles. J Hydrol. 1970;10(3):282-90.
[36] Gauch HG, Hwang JTG, Fick GW. Model evaluation by comparison of model predictions and observed values. Agron J. 2003;95(6):1442-6.

7. Appendix

Table 6 The raw data with Average (AVG), Standard Deviation (SD), Max and Min

No.	Dry Density					Moisture Content					MDD	OMC
Test	2%	4%	6%	8%	10%	2%	4%	6%	8%	10%		
1	1.3011	1.5813	1.6745	1.6176	1.5805	9.2233	11.33	12.5	14.5078	15.544	1.6745	12.5
2	1.054	1.4075	1.7455	1.3915	1.2127	8.9591	11.7927	14.2919	20.6675	22.6269	175%	14.2919
3	0.926	1.5975	1.8464	1.3074	1.1115	9.5206	12.8549	14.2381	18.1856	21.3229	185%	14.2381
4	1.2771	1.6361	1.8737	1.644	1.5026	8.4026	10.5059	14.1662	18.7085	21.9352	187%	14.1662
5	0.9761	1.3643	1.589	1.3585	1.2125	8.5294	12.7623	15.7447	18.6669	21.8957	159%	15.7447
6	1.0035	1.3336	1.5505	1.3156	1.1618	8.8797	12.6699	14.8111	18.382	20.0406	155%	14.8111
7	1.0641	1.5825	1.7615	1.5437	1.1561	8.501	12.3427	13.6881	16.6317	20.3101	1.7615	13.6881
8	0.9711	1.3548	1.5332	1.3774	1.1496	10.0675	13.8257	15.5464	20.1402	23.0404	1.5332	15.5464
9	1.2011	1.6059	1.8288	1.6315	1.506	8.8596	13.3877	16.4241	20.4728	22.4022	1.8288	16.4241
10	0.9234	1.5817	1.9552	1.578	1.1302	8.6005	11.2478	12.8403	16.466	18.2646	1.9552	12.8403
11	0.9995	1.4875	1.769	1.3768	1.2407	9.9891	13.9889	15.6165	19.4756	21.5359	1.769	15.6165
12	0.9819	1.481	1.7013	1.3449	1.1531	8.5964	13.8225	15.9992	20.41	22.7611	1.7013	15.9992
13	0.9974	1.3901	1.556	1.3017	1.1146	8.8404	13.853	15.3149	18.6418	23.1962	1.556	15.3149
14	0.9986	1.296	1.515	1.3229	1.1607	9.8257	13.2031	14.7705	20.0019	21.7362	1.515	14.7705
15	1.0228	1.37	1.7893	1.3125	1.1936	9.4803	12.5084	16.7434	20.2134	23.0257	1.7893	16.7434
16	0.9415	1.3357	1.5243	1.3239	1.1414	9.1705	13.0765	14.4694	17.6676	20.4885	1.5243	14.4694
17	1.0619	1.5983	1.9244	1.6144	1.1454	8.556	11.5368	13.4478	17.3758	20.8672	1.9244	13.4478
18	1.0243	1.4124	1.6787	1.334	1.1836	9.2154	12.1316	13.8321	16.8591	22.9208	1.6787	13.8321
19	1.1972	1.5352	1.7683	1.513	1.3227	8.5597	13.2828	15.2121	20.006	22.5374	1.7683	15.2121
20	1.1486	1.5363	1.9081	1.4911	1.2813	8.9654	11.1081	14.0432	16.443	21.5924	1.9081	14.0432
21	0.9869	1.4356	1.6719	1.3751	1.2397	9.1332	13.3317	15.6433	18.2374	23.2285	1.6719	15.6433
22	1.0331	1.6206	1.8824	1.5532	1.3205	8.4578	11.7475	13.1056	16.5407	17.8348	1.8824	13.1056
23	0.9856	1.4516	1.6946	1.4499	1.3273	9.8507	13.002	14.3603	16.7039	20.1158	1.6946	14.3603
24	1.0427	1.3608	1.6623	1.3782	1.2274	10.632	14.0546	15.6691	18.3465	23.2735	1.6623	15.6691
25	1.037	1.4203	1.5922	1.4031	1.2634	8.546	11.4004	13.4481	19.4	21.6688	1.5922	13.4481
26	1.0053	1.3055	1.5491	1.3098	1.1485	11.7184	14.6646	16.3502	20.0742	22.2173	1.5491	16.3502
27	0.9212	1.5677	1.9524	1.5802	1.4079	9.2254	11.3502	13.1772	17.9842	23.2562	1.9524	13.1772
28	0.965	1.395	1.73	1.3387	1.1193	8.562	12.8707	14.4333	17.1185	20.2722	1.73	14.4333
29	1.0742	1.5272	1.9006	1.2957	1.1838	9.0579	12.0531	13.6581	16.1222	20.4444	1.9006	13.6581
30	1.0455	1.3698	1.5372	1.3975	1.1248	8.7735	10.9522	17.2134	20.7495	22.8132	1.5372	17.2134
31	0.984	1.6492	1.9043	1.4777	1.2786	8.4688	13.5041	15.4242	19.4018	21.1716	1.9043	15.4242
32	1.1049	1.45	1.66	1.4544	1.3189	8.5848	12.4521	14.0204	20.7095	22.9726	1.66	14.0204
33	1.0484	1.3615	1.5302	1.2972	1.1662	10.0752	13.2882	16.1056	19.4355	23.0631	1.5302	16.1056
34	1.1901	1.6228	1.8284	1.4374	1.2516	8.5293	11.8257	14.8456	18.3337	21.8292	1.8284	14.8456
35	1.0047	1.6799	1.9467	1.3009	1.1337	9.3862	12.9364	14.8127	18.2001	21.6997	1.9467	14.8127
36	0.9154	1.5395	1.739	1.4554	1.2604	9.4516	11.648	13.0863	15.3496	22.6829	1.739	13.0863
37	0.9368	1.3227	1.6263	1.3213	1.14	8.6958	11.6355	15.5311	18.3203	23.0127	1.6263	15.5311
38	0.9716	1.3392	1.8706	1.3546	1.1749	11.0421	13.7116	15.6621	19.3535	21.5418	1.8706	15.6621
39	1.2924	1.6549	1.8737	1.4185	1.1307	8.671	13.2565	15.9838	20.214	23.2365	1.8737	15.9838
40	0.9571	1.4339	1.6124	1.3543	1.2364	10.6833	14.3711	15.9815	20.1553	23.0351	1.6124	15.9815
41	0.9575	1.3793	1.561	1.2959	1.1163	8.6285	11.2066	13.4549	16.6139	18.7585	1.561	13.4549
42	0.987	1.767	1.615	1.505	1.394	4.881	10.714	18.627	21.827	27.604	1.767	10.714
43	0.7996	1.5728	1.6835	1.2946	1.0696	4.7412	11.1515	21.2972	31.0944	40.1821	1.6835	21.2972
44	0.7024	1.7852	1.7807	1.2163	0.9804	5.0383	12.1559	21.217	27.3603	37.8665	1.7852	12.1559
45	0.9688	1.8283	1.807	1.5295	1.3253	4.4467	9.9347	21.1099	28.147	38.9537	1.8283	9.9347
46	0.7404	1.5246	1.5325	1.2639	1.0695	4.5138	12.0684	23.4621	28.0844	38.8836	1.5325	23.4621
47	0.7613	1.4903	1.4953	1.224	1.0247	4.6992	11.981	22.0709	27.6558	35.5892	1.4953	22.0709
48	0.8073	1.7684	1.6988	1.4362	1.0197	4.4988	11.6716	20.3975	25.0224	36.0678	1.7684	11.6716
49	0.7367	1.514	1.4787	1.2815	1.014	5.3277	13.074	23.1666	30.3011	40.9165	1.514	13.074
50	0.9112	1.7946	1.7637	1.5179	1.3283	4.6885	12.6598	24.4746	30.8014	39.7831	1.7946	12.6598

Table 6 (continued) The raw data with Average (AVG), Standard Deviation (SD), Max and Min

No.	Dry Density					Moisture Content					MDD	OMC
Test	2%	4%	6%	8%	10%	2%	4%	6%	8%	10%		
51	0.7005	1.7675	1.8857	1.4681	0.9968	4.5514	10.6363	19.1342	24.7732	32.4354	1.8857	19.1342
52	0.7582	1.6622	1.7061	1.2809	1.0943	5.2863	13.2283	23.271	29.3011	38.2447	1.7061	23.271
53	0.7449	1.655	1.6408	1.2513	1.0171	4.5492	13.0709	23.8414	30.7069	40.4205	1.655	13.0709
54	0.7566	1.5534	1.5007	1.2111	0.983	4.6784	13.0998	22.8217	28.0467	41.1931	1.5534	13.0998
55	0.7575	1.4482	1.4611	1.2308	1.0238	5.1998	12.4852	22.0104	30.0929	38.6003	1.4611	22.0104
56	0.7759	1.5309	1.7256	1.2212	1.0527	5.017	11.8283	24.9504	30.4112	40.8903	1.7256	24.9504
57	0.7142	1.4926	1.4701	1.2317	1.0067	4.8531	12.3655	21.5617	26.581	36.3847	1.4926	12.3655
58	0.8056	1.7861	1.856	1.502	1.0102	4.5278	10.9095	20.0394	26.142	37.0572	1.856	20.0394
59	0.7771	1.5783	1.619	1.2412	1.044	4.8768	11.472	20.612	25.3646	40.704	1.619	20.612
60	0.9082	1.7156	1.7054	1.4076	1.1666	4.5298	12.5606	22.6684	30.0992	40.0231	1.7156	12.5606
61	0.8713	1.7168	1.8403	1.3873	1.1301	4.7445	10.5041	20.9266	24.7385	38.345	1.8403	20.9266
62	0.7486	1.6043	1.6124	1.2794	1.0935	4.8333	12.6068	23.3111	27.4383	41.2506	1.6124	23.3111
63	0.7837	1.811	1.8154	1.4451	1.1647	4.4759	11.1088	19.5294	24.8855	31.6721	1.8154	19.5294
64	0.7477	1.6221	1.6344	1.3489	1.1707	5.213	12.2951	21.3992	25.1311	35.7229	1.6344	21.3992
65	0.791	1.5207	1.6032	1.2823	1.0826	5.6265	13.2905	23.3494	27.6024	41.3305	1.6032	23.3494
66	0.7866	1.5871	1.5355	1.3054	1.1144	4.5226	10.7806	20.0398	29.1874	38.4806	1.5871	10.7806
67	0.7627	1.4588	1.494	1.2186	1.013	6.2014	13.8672	24.3643	30.2017	39.4547	1.494	24.3643
68	0.6988	1.7518	1.8829	1.4702	1.2418	4.8821	10.733	19.6361	27.0573	41.2998	1.8829	19.6361
69	0.7321	1.5588	1.6685	1.2455	0.9872	4.531	12.1709	21.5079	25.7549	36.0005	1.6685	21.5079
70	0.8149	1.7066	1.833	1.2055	1.0441	4.7935	11.3977	20.3527	24.2559	36.3064	1.833	20.3527
71	0.7932	1.5308	1.4826	1.3002	0.9921	4.643	10.3567	25.6507	31.2177	40.513	1.5308	10.3567
72	0.7465	1.843	1.8366	1.3748	1.1277	4.4817	12.7698	22.9845	29.19	37.5977	1.843	12.7698
73	0.8382	1.6203	1.6009	1.3531	1.1633	4.5431	11.7751	20.8927	31.1576	40.7961	1.6203	11.7751
74	0.7953	1.5214	1.4758	1.2069	1.0286	5.3318	12.5657	23.9999	29.2408	40.9568	1.5214	12.5657
75	0.9028	1.8135	1.7634	1.3373	1.1039	4.5137	11.1827	22.1223	27.5831	38.7655	1.8135	11.1827
76	0.7622	1.8773	1.8774	1.2103	0.9999	4.9672	12.233	22.0733	27.3821	38.5356	1.8774	22.0733
77	0.6945	1.7204	1.6772	1.354	1.1117	5.0018	11.0147	19.5006	23.0936	40.2816	1.7204	11.0147
78	0.7106	1.4781	1.5685	1.2293	1.0055	4.6018	11.0029	23.1438	27.563	40.8673	1.5685	23.1438
79	0.7371	1.4965	1.8041	1.2603	1.0363	5.8435	12.9661	23.3391	29.1175	38.2551	1.8041	23.3391
80	0.9804	1.8493	1.807	1.3197	0.9973	4.5887	12.5357	23.8184	30.412	41.2648	1.8493	12.5357
81	0.726	1.6023	1.5551	1.26	1.0905	5.6536	13.5897	23.8151	30.3237	40.907	1.6023	13.5897
82	0.7263	1.5414	1.5055	1.2057	0.9846	4.5662	10.5972	20.0499	24.9956	33.3124	1.5414	10.5972
83	1.2422	1.4728	1.6	1.5196	1.4361	14.2857	16.2791	18.3432	21.8935	27.1605	1.6	18.3432
84	1.0063	1.311	1.6679	1.3072	1.1019	13.8764	16.9438	20.9727	31.1891	39.5365	1.6679	20.9727
85	0.8841	1.488	1.7642	1.2281	1.01	14.7461	18.4699	20.8937	27.4436	37.2581	1.7642	20.8937
86	1.2194	1.5239	1.7903	1.5444	1.3653	13.0145	15.0949	20.7883	28.2328	38.3278	1.7903	20.7883
87	0.9319	1.2708	1.5183	1.2762	1.1018	13.2109	18.337	23.1046	28.17	38.2589	1.5183	23.1046
88	0.9581	1.2422	1.4815	1.2359	1.0557	13.7535	18.2042	21.7346	27.74	35.0174	1.4815	21.7346
89	1.016	1.474	1.6831	1.4502	1.0505	13.167	17.7341	20.0868	25.0986	35.4883	1.6831	20.0868
90	0.9272	1.2619	1.465	1.2939	1.0446	15.5932	19.8649	22.8136	30.3934	40.2591	1.465	22.8136
91	1.1468	1.4958	1.7474	1.5327	1.3685	13.7224	19.2355	24.1017	30.8952	39.1439	1.7474	24.1017
92	0.8816	1.4733	1.8682	1.4824	1.027	13.3212	16.1609	18.8426	24.8486	31.9142	1.8682	18.8426
93	0.9543	1.3855	1.6903	1.2933	1.1273	15.4719	20.0993	22.9165	29.3904	37.6303	1.6903	22.9165
94	0.9375	1.3794	1.6256	1.2634	1.0478	13.3147	19.8602	23.4782	30.8005	39.771	1.6256	23.4782
95	0.9523	1.2948	1.4867	1.2228	1.0127	13.6927	19.9041	22.474	28.1321	40.5313	1.4867	22.474
96	0.9534	1.2071	1.4475	1.2427	1.0547	15.2187	18.9703	21.6751	30.1846	37.9801	1.4475	21.6751
97	0.9765	1.2761	1.7096	1.233	1.0845	14.6838	17.9722	24.5702	30.5038	40.2333	1.7096	24.5702
98	0.8989	1.2441	1.4565	1.2436	1.0371	14.204	18.7883	21.2332	26.6619	35.8001	1.4565	21.2332
99	1.0139	1.4887	1.8388	1.5166	1.0407	13.2521	16.5761	19.7341	26.2216	36.4618	1.8388	19.7341
100	0.978	1.3155	1.604	1.2532	1.0755	14.2735	17.4308	20.298	25.4418	40.05	1.604	20.298
101	1.1431	1.43	1.6896	1.4213	1.2019	13.2578	19.0848	22.323	30.1908	39.3801	1.6896	22.323
102	1.0966	1.431	1.8232	1.4008	1.1642	13.8863	15.9602	20.6077	24.8139	37.729	1.8232	20.6077
103	0.9422	1.3372	1.5975	1.2918	1.1265	14.1461	19.1551	22.9559	27.5219	40.5878	1.5975	22.9559
104	0.9863	1.5095	1.7986	1.4591	1.1999	13.1	16.8789	19.2319	24.9613	31.1632	1.7986	19.2319
105	0.941	1.3521	1.6192	1.362	1.206	15.2574	18.6814	21.0731	25.2077	35.1489	1.6192	21.0731
106	0.9955	1.2675	1.5884	1.2947	1.1153	16.4677	20.1938	22.9937	27.6865	40.6664	1.5884	22.9937
107	0.99	1.3229	1.5213	1.3181	1.148	13.2367	16.3802	19.7344	29.2764	37.8624	1.5213	19.7344
108	0.9599	1.216	1.4802	1.2304	1.0436	18.1503	21.0702	23.9931	30.2938	38.8208	1.4802	23.9931
109	1.2103	1.3869	1.6005	1.2742	1.061	13.468	16.7179	22.791	27.6464	40.2099	1.6005	22.791
110	1.2554	1.4042	1.841	1.3063	1.0935	17.1019	19.7009	22.9833	29.2055	37.6398	1.841	22.9833
111	1.6697	1.7353	1.8439	1.368	1.0524	13.4295	19.0469	23.4552	30.504	40.6011	1.8439	23.4552
112	1.2365	1.5035	1.5869	1.306	1.1508	16.5462	20.6484	23.452	30.4154	40.249	1.5869	23.452
113	1.237	1.4463	1.5363	1.2497	1.039	13.3637	16.1016	19.7442	25.0712	32.7765	1.5363	19.7442
114	1.1464	1.5155	1.7315	1.2998	1.0756	10.9666	19.4141	23.2634	28.4801	44.5978	1.7315	23.2634
115	0.985	1.4162	1.5171	1.1987	1.0407	11.1718	23.3004	25.9142	31.5882	47.9771	1.5171	25.9142
116	1.0311	1.5987	1.7081	1.354	1.1085	10.3456	20.5316	21.7103	28.6493	36.8367	1.7081	21.7103
117	0.9837	1.4319	1.5377	1.2639	1.1142	12.0494	22.7242	23.7888	28.932	41.548	1.5377	23.7888
118	1.0407	1.3424	1.5084	1.2014	1.0303	13.0052	24.5639	25.9568	31.7771	48.0701	1.5084	25.9568
119	1.035	1.401	1.4447	1.2231	1.0606	10.4536	19.925	22.2776	33.6019	44.7555	1.4447	22.2776
120	1.0034	1.2878	1.4057	1.1417	0.9641	14.3341	25.6299	27.0851	34.7696	45.8884	1.4057	27.0851
AVG	0.9547	1.5065	1.6745	1.3497	1.1381	9.1910	14.3878	19.5967	24.8372	32.7768	1.6812	17.8943
SD	0.1644	0.1586	0.1425	0.1127	0.1214	3.7954	3.5089	3.8480	5.1238	8.6169	0.1409	4.5020
Max	1.6697	1.8773	1.9552	1.644	1.5805	18.1503	25.6299	27.0851	34.7696	48.0701	1.9552	27.0851
Min	0.6945	1.2071	1.4057	1.1417	0.9641	4.4467	9.9347	12.5	14.5078	15.544	1.4057	9.9347

Remark: The percentages of 2%, 4%, 6%, 8%, and 10% represent the amounts of moisture content added, based on the guidelines of ASTM D1557.